IET Signal Processing

Research Article

IET Journals
The Institution of Engineering and Technology

Automated system for weak periodic signal detection based on Duffing oscillator

ISSN 1751-9675
Received on 29th April 2020
Revised 7th December 2020
Accepted on 8th December 2020
E-First on 16th February 2021
doi: 10.1049/iet-spr.2020.0203
www.ietdl.org

Mahmut Akilli[1] ✉, *Nazmi Yilmaz*[2], *Kamil Gediz Akdeniz*[3]

[1]*Istanbul Atlas University, Vocational School, Istanbul, Turkey*
[2]*Koç University, College of Sciences, Department of Physics, Istanbul, Turkey*
[3]*Disordered Systems Working Group, Istanbul, Turkey*
✉ *E-mail: akillimahmut@yahoo.com.tr*

Abstract: The periodic signals that have predictable and deterministic characteristics are used in the analysis and modelling of dynamical systems in diverse fields. These signals can be detected as the weak signals within the time series obtained from the measurable processes of dynamical systems. The Duffing oscillator is effective in detecting weak periodic signals with a very low signal-to-noise ratio. In this study, the authors present a method to automate the weak periodic signal detection of the Duffing oscillator using a quantitative index for the classification of the periodic and non-periodic signals. In this method, the authors use the wavelet scale index as the quantitative index in the classification of signals. Thus, they are able to plot the wavelet scale index spectrum of the Duffing oscillator where the frequency values of the weak periodic signals correspond to near-zero wavelet scale index parameters. First, the authors perform simulations using the method and detect weak periodic signals embedded in noise. Then, they employ two electroencephalogram signals to demonstrate the feasibility of the proposed method in the empirical data. Lastly, they compare the method to the periodogram power spectral density estimate based on fast Fourier transform.

1 Introduction

The periodic or quasi-periodic signals can be detected as the weak signals in the time series obtained from the measurable processes of dynamical systems such as electroencephalogram (EEG) signals in the brain [1–3] and seismic signals in earthquakes [4–6]. The weak periodic signals [7–10] have a very low signal-to-noise ratio (SNR), thus, have low amplitudes. The weak periodic signals that have predictable and deterministic characteristics are used in the analysis of the dynamical systems, especially in the processing of non-stationary signals in various applications such as the development of biomedical device technology.

The Duffing oscillator is widely used for the detection of weak periodic signals in intense noise. The weak periodic signals within the external forcing input term in the Duffing oscillator are detected by observing the transition of the oscillator from a chaotic state to periodic state. When the Duffing oscillator, in the critical edge of chaos, is stimulated by the weak periodic signals embedded in strong background noise, the Duffing oscillator jumps to a periodic state [11–20]. This conventional method of detecting weak periodic signals is based on analysing the change in the state space of the Duffing oscillator manually which is not practical and time-consuming. In this study, we propose a new method to automate the detection of weak periodic signals, based on the wavelet scale index which numerically identifies the state transition of the Duffing oscillator.

The wavelet scale index is a recently introduced method, based on the wavelet analysis. It is used for measuring the degree of non-periodicity of a signal [21, 22]. One can numerically separate the periodic and non-periodic states of the Duffing oscillator using the wavelet scale index [23–26]. Hence, the classification of the periodic and non-periodic signals by the wavelet scale index allows the conventional method to be automated in practice. Thus, the wavelet scale index will allow performing the weak periodic signal search without the need to manually analyse the state space diagrams of the Duffing oscillator.

In this paper, we apply this automated method to detect weak periodic signals embedded in noise and in empirical signals. For this, the signals are used as external forcing input in the Duffing oscillator. Then, the wavelet scale index method is computed from the time series of an array of Duffing oscillators. The paper is organised as follows. In Section 2.2, we justify using the wavelet scale index as the quantitative index in the weak periodic signal detection. Thus, we analyse the wavelet scale index spectrum of the Duffing oscillator and compare the results with a different quantitative index, the maximum Lyapunov exponent. We show that the wavelet scale index is more effective than the maximum Lyapunov exponent in the detection of the transition to the periodic state from the critical edge of chaos for the Duffing oscillator. As the wavelet scale index parameter goes to zero in every periodic-stable state of the Duffing oscillator. In Section 3, we explain the application of the proposed method in detail. In Section 3.1, we test and verify the method by performing simulations where the results demonstrate the capability of this automated method for detecting weak periodic signals embedded in noise. We also compare the graphical results obtained with the method to the periodogram power spectral density estimate based on fast Fourier transform (FFT). Furthermore, in Section 3.2, we describe the application to the empirical data where we carry out the proposed method of weak periodic signal detection effectively in EEG signals.

Data: EEG signals used in this work were obtained from two patients; the EEG data was approved by Celal Bayar University Medical Faculty Ethics Committee in 2009.

2 Theoretical basis

2.1 Detection method of weak periodic signals by utilising the Duffing oscillator

Duffing equation, in its simple form, can be expressed as [11, 15, 20, 27, 28]:

$$\frac{\mathrm{d}^2x}{\mathrm{d}t^2} + 0.5\frac{\mathrm{d}x}{\mathrm{d}t} - x + x^3 = \gamma\cos(t) + \text{input} \tag{1}$$

where $\gamma\cos(t)$ is the reference signal with the amplitude γ. The 'input' term represents the external forcing input to the oscillator. Weak periodic signals within the input signal are low amplitude

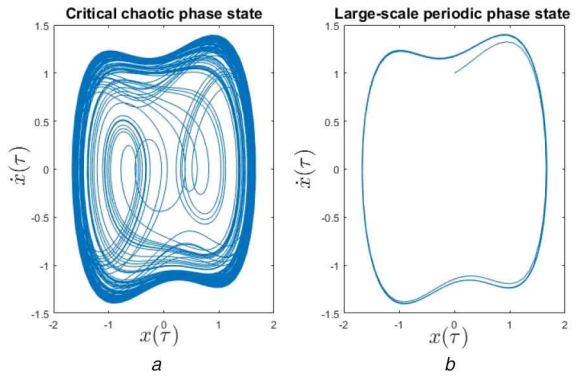

Fig. 1 *State space of the Duffing oscillator system without external forcing input*

(a) Oscillator is in the critical chaotic state space for the amplitude value of $\gamma = 0.825$, ***(b)*** Oscillator jumps into a large-scale stable-periodic state for the amplitude value of $\gamma_c = 0.826$

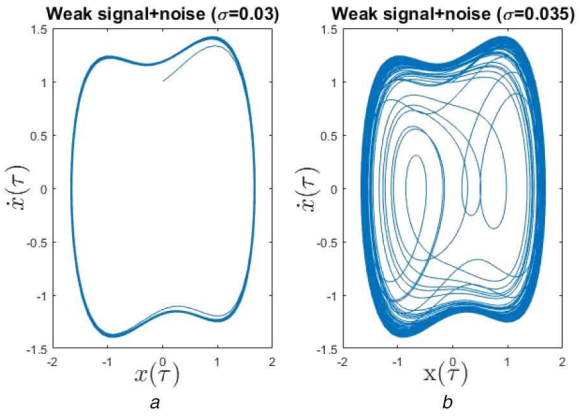

Fig. 2 *Measuring the high sensitivity of the Duffing oscillator in the detection of the weak periodic signals with very low SNR*

(a) Large scale stable-periodic state of the oscillator is maintained for $\boldsymbol{\sigma} = 0.03$, ***(b)*** Large scale stable-periodic state of the oscillator is deformed for $\boldsymbol{\sigma} = 0.035$.

signals in comparison to the reference signal [11, 15, 23]. Wang *et al.* [11] first described the conventional method of detecting weak periodic signals within the signals that are used as external forcing input in the Duffing equation. In this conventional method, the state-space diagrams are plotted manually to detect the transition of the Duffing oscillator from a chaotic state to a periodic state.

For the weak periodic signal detection, frequency transformation is performed by changing the frequency of the reference signal in (1). Assuming $y = \mathrm{d}x(t)/\mathrm{d}t = \dot{x}(t)$, the time variable in (1) is defined as $t = \omega_0\tau$, where ω_0 is the reference angular frequency. Therefore (1) yields [11]:

$$\frac{\mathrm{d}x}{\mathrm{d}\tau} = \dot{x}(\tau) = \omega_0 y \tag{2}$$

$$\frac{\mathrm{d}y}{\mathrm{d}\tau} = \dot{y}(\tau) = \omega_0\left[-0.5y + x - x^3 + \gamma\cos(\omega_0\tau) + \mathrm{input}(\tau)\right]$$

The input signal can be defined as

$$\mathrm{input}(\tau) = s(\tau) + n(\tau) \tag{3}$$

where $n(\tau)$ is the noise. Let us assume $s(\tau) = a\cos(\omega\tau)$ is the weak periodic signal, where ω is the angular frequency and a is the amplitude of the weak periodic signal.

The numerical solutions of the Duffing (2) can be acquired by the fourth-order Runge–Kutta method [29], using a time step size of $h = 0.1$ for $0 \le \tau \le i \cdot h$, where i is the iteration number, and the initial values of $x(0) = 0$ and $\dot{x}(0) = 1$. The state space is plotted for the numerical solutions, $x(\tau)$, and the derivatives of the numerical solutions, $\dot{x}(\tau)$.

The period of the orbits in a large-scale periodic state space of the Duffing oscillator is $T = 100$ [11, 12], $0 \le \tau \le mT$ ($m = 1, 2, 3, \ldots$). The sampling frequency of the discrete Duffing oscillator is determined as $f_D = 100/h$. For example, when the step size is selected as $h = 0.1$, the sampling frequency of the Duffing oscillator, f_D is calculated as 1000 Hz. Since the cosine function is a double function, the weak periodic signal search of the Duffing oscillator can only be possible in the frequency range of 0–500 Hz. Generally, the weak periodic signal search on the frequency domain is performed by adjusting the sampling frequency of the Duffing oscillator, f_D.

The Duffing oscillator without the external forcing input remains in a large-scale periodic state if the amplitude (γ) of the reference signal is greater than or equal to the bifurcation value, γ_c [11, 12]. For detecting a weak periodic signal embedded in noise, the amplitude of the reference signal (γ) is adjusted to the critical chaotic state space of the Duffing oscillator as shown in Fig. 1*a* before including the input signal in (2). Then, the reference amplitude (γ) is fixed and the angular frequency of the reference signal (ω_0) is changed for the frequency scanning. In the case that the total periodic amplitude in (2) is $\gamma + a \ge \gamma_c$; the Duffing oscillator only goes to periodic-stable state as shown in Fig. 1*b*, when the angular frequency of the reference signal and the periodic signal in the input term is equal to each other ($\omega = \omega_0$) [11–15, 27].

Fig. 1*a* shows the critical chaotic state space of the Duffing oscillator without the external forcing input for $\gamma = 0.825$, $\omega_0 = 1$ and $h = 0.1$. When the reference amplitude (γ) in the critical chaotic state is increased by 0.001, the oscillator leaps to a large-scale periodic state for $\gamma_c = 0.826$ as shown in Fig. 1*b*. The bifurcation value for the reference signal, γ_c depends on its angular frequency, ω_0 and the step size, $h = 100/f_D$.

We used Matlab in all applications in this work. We performed a simulation to demonstrate the high sensitivity of the Duffing oscillator for the detection of weak periodic signals with very low SNR [11–15, 23].

Thus, we added the input signal term in (3) while the oscillator is in a critical chaotic state for $\gamma = 0.825$, as shown in Fig. 1*a*. As a result, the Duffing oscillator jumped to a periodic-stable state as shown in Fig. 2*a*. In the simulation, the weak periodic signal term was determined as $s(\tau) = 0.001\cos(\omega\tau)$, with $\omega = \omega_0 = 1$. The noise term was determined as $n(\tau) = \sigma \cdot \mathrm{rand}n(\tau)$; where $\mathrm{rand}n(\tau)$ is a Matlab function which produces a normally distributed random number with 0 mean and variance 1 for each time τ. σ is the noise multiple which was selected as 0.03 and 0.035, respectively as shown in Fig. 2. The results in Fig. 2 show that the reliable weak periodic signal detection is possible only when $\sigma \le 0.03$. Therefore, the SNR threshold for the analysed signal must be higher than -32.55 db

$$\mathrm{SNR} = 10\log_{10}\left(0.5\frac{a^2}{\sigma^2}\right) = 10\log_{10}\left(0.5\frac{(0.001)^2}{(0.03)^2}\right) = -32.55 \ \mathrm{db} \tag{4}$$

2.2 Wavelet scale index analysis of the Duffing oscillator

The wavelet scale index was first presented by Benitez *et al.* [21, 22]. It gives quantitative information on the level of non-periodicity of signals. The wavelet scale index is based on the continuous wavelet transform (CWT). The CWT of a function $f(t)$ is formulated as [30]

$$Wf(u,s) = \langle f, \psi_{u,s} \rangle = \int_{-\infty}^{+\infty} f(t)\psi^*_{u,s}(t)\mathrm{d}t \tag{5}$$

The CWT allows us to obtain the frequency components of the function $f(t)$ corresponding to scale s and time location u, thus providing a time–frequency decomposition of $f(t)$.

The scalogram function of $f(t)$, is defined as:

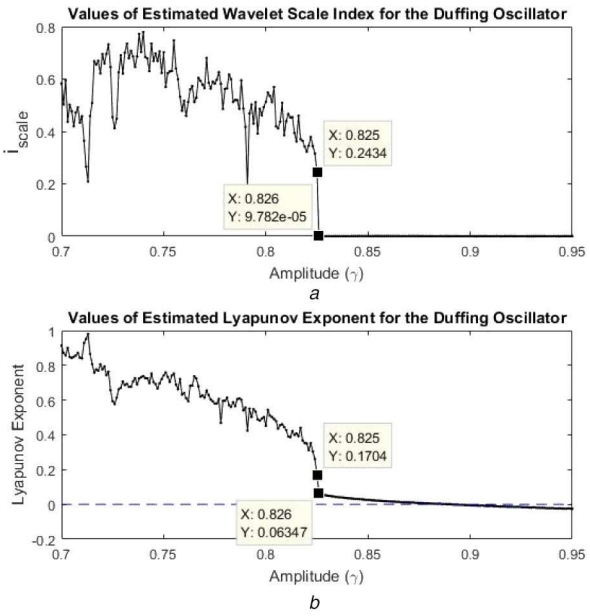

Fig. 3 *Duffing oscillator without external forcing input stays in the periodic state for the reference amplitude values of* $\gamma \geq \gamma_c = 0.826$

(a) Wavelet scale index spectrum of the Duffing oscillator. The wavelet scale index parameters converge to zero for the amplitude values of $\gamma \geq \gamma_c = 0.826$, $i_{\text{scale}} \to 0$, ***(b)*** Maximum Lyapunov exponent spectrum of the Duffing oscillator. The maximum Lyapunov exponent takes zero or negative values for the amplitude values of $\gamma > 0.891$

$$S(s) = Wf(u,s) = \left(\int_{-\infty}^{+\infty} |Wf(u,s)|^2 \mathrm{d}u \right)^{1/2} \tag{6}$$

Here, the scalogram function represents the energy of the CWT of $f(t)$ at each scale. For the signal f to be analysed in practical terms, a finite time interval must be considered. Therefore, the inner scalogram of the signal f at s scale is written as [21]:

$$S^{\text{inner}}(s) = Wf(u,s)_{J(s)} = \left(\int_{c(s)}^{d(s)} |Wf(u,s)|^2 \mathrm{d}u \right)^{1/2} \tag{7}$$

Here $J(s) = [c(s),\ d(s)]$ is the maximum subinterval in the finite time interval where the wavelet function is supported. To achieve a wavelet scale index parameter independent of the scale, the inner scalogram is normalised as follows [21]:

$$\bar{S}^{\text{inner}}(s) = \frac{S^{\text{inner}}(s)}{(d(s) - c(s))^{1/2}} \tag{8}$$

The definition of the wavelet scale index of a signal at scale range $[s_0, s_1]$ is

$$i_{\text{scale}} = \frac{\bar{S}^{\text{inner}}(s_{\min})}{\bar{S}^{\text{inner}}(s_{\max})} \tag{9}$$

where $s_{\max}$ is the smallest scale that gives the normalised inner scalogram its maximum value between the scales of s_0 and s_1. In addition, $s_{\min}$ is the smallest scale that gives the normalised inner scalogram its minimum value between the scales of $s_{\max}$ and $2s_1$. The wavelet scale index parameters can vary between zero and one, $0 \leq i_{\text{scale}} \leq 1$. When the computed wavelet scale index parameter is zero or very close to zero, it indicates that the signal is periodic. Also, when the wavelet scale index parameter is close to one, it refers that the signal is highly non-periodic [21, 22].

We calculated the wavelet scale index parameter from the time series of $x(\tau)$ that were obtained from the solutions of the Duffing equation with no external forcing input. Fig. 3*a* shows the wavelet scale index spectrum of the Duffing chaotic oscillator, plotted by fixing ω as $\omega_0 = 1$ and changing the amplitude (γ) of the reference signal by the increment of 0.001 in the range of 0.700 and 0.950. The wavelet function of Haar with the scale range of $s_0 = 1$ and $s_1 = 512$ was used for computing the wavelet scale index parameters. Fig. 3*a* shows that the wavelet scale index parameters converge to zero when the system stays in the periodic state for $\gamma \geq 0.826$. In addition, the wavelet scale index parameters are higher than zero when the system is in the chaotic state for $\gamma \leq 0.825$. Hence, the wavelet scale index method is capable of numerically identifying the transition between chaotic and periodic states of the oscillator. Since the wavelet scale index parameters converge to zero in all periodic oscillators, the method can distinguish periodic signals from non-periodic or chaotic signals.

The maximum Lyapunov exponent (λ) quantitatively determines whether the system is chaotic ($\lambda > 0$) or periodic ($\lambda \leq 0$). Therefore, the state spaces of the Duffing chaotic oscillator can also be identified numerically by the maximum Lyapunov exponent [31, 32]. However, as shown in Fig. 3, the maximum Lyapunov exponent is not as sensitive as the wavelet scale index in the detection of the transition to the periodic state from the critical edge of chaos in the Duffing oscillator. The values of the estimated maximum Lyapunov exponent for the periodic region are zero or negative, $\lambda \leq 0$, However, for $\gamma_c = 0.826$, the maximum Lyapunov exponent value is slightly above zero, $\lambda_c = 0.06347$. Therefore, the method lacks sensitivity during the transition of the oscillator from the chaotic state to the periodic state. For this reason, we preferred the wavelet scale index instead of the maximum Lyapunov exponent as a quantitative index in detecting weak periodic signals.

3 Proposed method

3.1 Weak periodic signal detection by the wavelet scale index spectrum of the duffing oscillator

In conventional weak periodic signal detection practices, weak periodic signals with unknown frequency values in an input signal are identified by observing the transition of the Duffing oscillator from a chaotic state to a periodic state. For this, the state space diagrams of the oscillator are analysed by manually sweeping the angular frequency (ω_0) of the reference signal in (2) [11–20, 27], which is evidently impractical. We devised an effective method to improve the existing process using the wavelet scale index analysis of the Duffing oscillator.

The wavelet scale index method enables us to distinguish the periodic states from the non-periodic states by quantitative means. As near-zero wavelet scale index values indicate the periodic oscillations of the system, $i_{\text{scale}} \to 0$. If the Duffing oscillator jumps to a periodic-stable state, the wavelet scale index of the Duffing oscillator will be very close to zero. Hence, a weak periodic signal with an unknown frequency can be detected simply by tracking the values of the wavelet scale index–frequency graph. This method of combining the wavelet scale index and the Duffing oscillator proves to be more effective in searching weak periodic signals compared to plotting the state space of the Duffing oscillator for each frequency. The weak periodic signals can be detected by using the wavelet scale index–frequency spectrum graph of the Duffing oscillator, similar to FFT. Here, the frequency values of the weak periodic signals correspond to near-zero values of the wavelet scale index in the spectrum graph. Therefore, the proposed method will automatically search weak periodic signals without the need to analyse the state space diagrams of the Duffing oscillator. The simulation example of the proposed method is given below.

The weak periodic signals were formed from a T-periodic function, $\tau \in [0, T]$, $s(\tau) = \sum_{n=1}^{N} A_n \cos(2\pi f_n \tau / T)$. Where A_n is the signal's nth amplitude, f_n is the signal's nth frequency. The time step size h was used to obtain a discrete signal from the continuous $s(\tau)$ function, $0 \leq \tau \leq i \,.\, h$, where i is the iteration number. Here, the sampling frequency of the discrete $s[\tau]$ function was calculated as $f_s = T/h$.

Fig. 4*a* shows the weak periodic signals (10) with frequency values of 10, 17, 25 and 35 Hz in the period, $T = 100$. For the discrete time τ, the time step size, $h = 0.1$ and the iteration, $i = 10,000$ was used

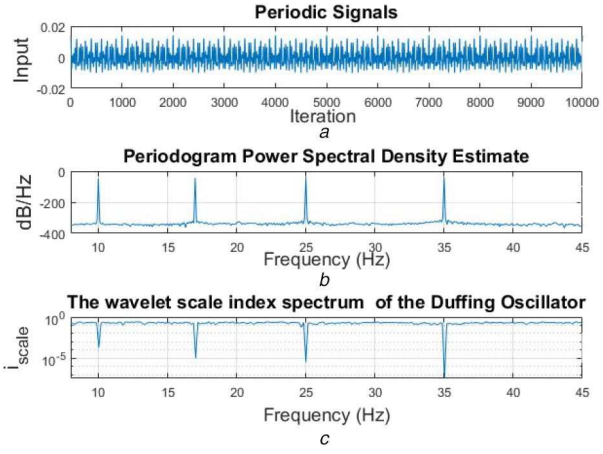

Fig. 4 *Wavelet scale index spectrum of the Duffing oscillator system with external forcing input signal, and periodogram power spectral density of the input signal*

(a) Input(τ) represents the weak periodic signals with the frequency values of 10, 17, 25 and 35 Hz, ***(b)*** Periodogram power spectral density estimate for the input signal, ***(c)*** Wavelet scale index spectrum of the Duffing oscillator: the frequency values of the weak periodic signals that are used as external forcing input in the Duffing equation correspond to near-zero wavelet scale index parameters in the graph

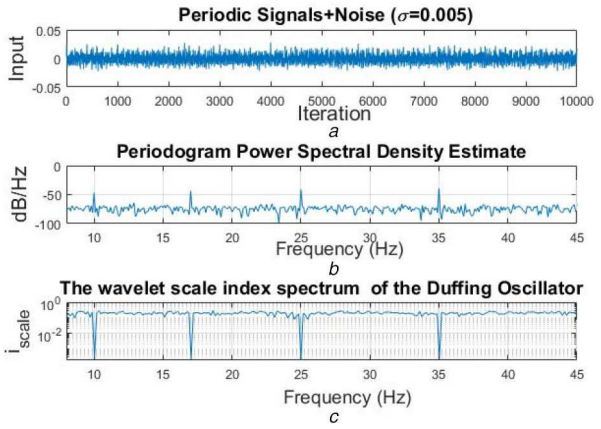

Fig. 5 *Wavelet scale index spectrum of the Duffing oscillator system with external forcing input signal, and periodogram power spectral density of the input signal*

(a) Input(τ) represents the weak periodic signals in intense noise with the frequency values of 10, 17, 25 and 35 Hz, $\sigma = 0.005$, ***(b)*** Periodogram power spectral density estimate for the input signal, ***(c)*** Wavelet scale index spectrum of the Duffing oscillator: the frequency values of the weak periodic signals that are used as external forcing input in the Duffing equation correspond to near-zero wavelet scale index parameters in the graph

$$s[\tau] = 0.002\cos\left(2\pi 10\frac{\tau}{100}\right) + 0.003\cos\left(2\pi 17\frac{\tau}{100}\right) + 0.004\cos\left(2\pi 25\frac{\tau}{100}\right) + 0.005\cos\left(2\pi 35\frac{\tau}{100}\right) \quad (10)$$

Input signal, $\text{input}[\tau] = s[\tau] + n[\tau]$, consists of the weak periodic signals submerged in noise. $n[\tau] = \sigma \,.\, \text{rand}n(\tau)$, is the noise term where rand$n(\tau)$ is a Matlab function which produces a normally distributed random number with 0 mean and variance 1 for each time τ. σ is the noise multiplier. Figs. 5*a* and 6*a* show the input signals consisting of the weak periodic signals and the noise for $\sigma = 0.005$ and $\sigma = 0.03$, respectively.

$$\frac{\mathrm{d}^2x}{\mathrm{d}t^2} + 0.5\frac{\mathrm{d}x}{\mathrm{d}t} - x + x^3 = 0.825\cos(\omega_0\tau) + \text{input}[\tau] \quad (11)$$

Frequency values of the weak periodic signals were detected automatically within these signals that are used as external forcing input in the Duffing (11). For this, the frequency scanning was carried out in the range of $0.50 \le \omega_0 \le 2.83$ ($7.96\,\text{Hz} \le f \le 45.1\,\text{Hz}$). The wavelet scale index was applied to the time series of $x(\tau)$ that were obtained from (11) by fixing the reference amplitude to $\gamma = 0.825$. Here, the wavelet function of Haar with the scale range of $s_0 = 1$ and $s_1 = 512$ was used for these calculations. Figs. 4*c*, 5*c* and 6*c* show the wavelet scale index spectrum of the Duffing oscillator for this frequency scanning. The wavelet scale index parameters closest to zero show the presence of weak periodic signals within the input signal. The weak periodic signals detected by this method can be observed in Figs. 4*c*, 5*c* and 6*c*. The method was also compared with the power spectra which can hardly detect weak periodic signals with low noise ($\sigma = 0.005$) as shown in Fig. 5*b* and appears short of detecting weak periodic signals in high noise ($\sigma = 0.03$) as shown in Fig. 6*b*.

As demonstrated in Fig. 7, in the weak periodic signal detection, the sampling frequency of the oscillator, f_D must be equal to the sampling frequency of the input signal, f_input. As $x(\tau)$, $\cos(\omega_0\tau)$ and input[τ] are dependent on τ in the Duffing (11), $0 \le \tau \le i\,.\,h$, where h is the time step size, and i is the iteration number. Here, to provide equality, $f_\text{input} = f_\text{D} = 100/h$, the time step size of the Duffing oscillator was determined as $h = 100/f_\text{input}$.

The input signal in (12) was formed by the weak periodic signals with frequency values of 8, 12 and 14 Hz, under the conditions that $T = 200$, $h = 0.4$ and $i = 5000$. The sampling frequency of the input signal was calculated as $f_\text{input} = 200/0.4 = 500$ Hz.

$$\text{input}[\tau] = 0.001\cos\left(2\pi 8\frac{\tau}{200}\right) + 0.002\cos\left(2\pi 12\frac{\tau}{200}\right) + 0.003\cos\left(2\pi 14\frac{\tau}{200}\right) \quad (12)$$

Fig. 7*a* shows the time series of the input signal with the sampling frequency of $f_\text{input} = 500$ Hz. The time step size of the Duffing oscillator was determined as $h = 100/f_\text{input} = 100/500 = 0.2$, and the sampling frequency of the Duffing oscillator was calculated as $f_\text{D} = 100/0.2 = 500\,\text{Hz}$. Fig. 7*b* shows the weak periodic signals detected by the Duffing oscillator with the sampling frequency of $f_\text{D} = 500$ Hz. When the sampling frequency of the Duffing oscillator was increased to $f_\text{D} = 1000$ Hz, $h = 100/f_\text{D} = 100/1000 = 0.1$, the weak periodic signal detection was not successful as shown in Fig. 7*c*.

3.2 Detecting weak periodic signals in the empirical data

In this section, the experimentally measured time series of a signal were used as external forcing input in the Duffing (2). First, this empirical data was multiplied with a suitable gain coefficient (10^n, $n = \ldots -2, -1, 0, 1, 2\ldots$) to scale the amplitude of the input signal to the reference signal [15, 23]. As the Duffing oscillator collapses when the amplitude magnitudes of the input signal are too large compared to the reference signal, and the Duffing oscillator is not stimulated when the amplitude magnitudes are too small. The root mean square (rms) of the signals were calculated to determine the gain coefficient for the condition of $10^n(\text{input})_\text{rms} < \gamma(\cos(\omega_0\tau))_\text{rms}$. For the EEG signals that we used as the empirical data in this work, the limit of the scaling was expressed as

$$0.01 < \frac{10^n(\text{input})_\text{rms}}{0.707\gamma} < 0.1 \quad (13)$$

Second, the sampling frequency of the Duffing oscillator was set equal to the sampling frequency of the input signal, $f_\text{D} = f_\text{input}$. As a result, the step size of the Duffing oscillator was determined as $h = 100/f_\text{input}$.

EEG signals recorded by the electrodes placed on the scalp are known to be contaminated by various types of background noise.

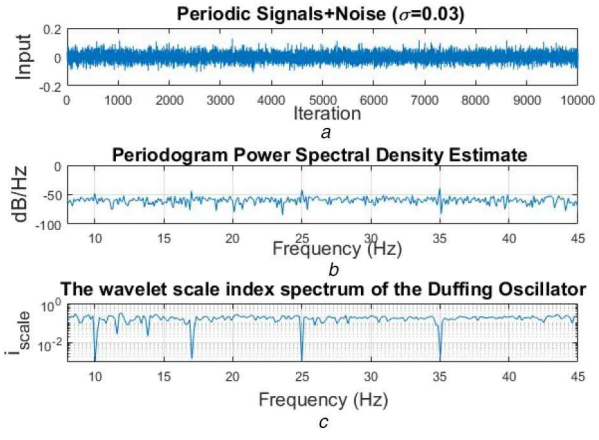

Fig. 6 *Wavelet scale index spectrum of the Duffing oscillator system with external forcing input signal, and periodogram power spectral density of the input signal*

(a) Input(τ) represents the weak periodic signals in intense noise with the frequency values of 10, 17, 25 and 35 Hz, $\sigma = 0.03$, ***(b)*** Periodogram power spectral density estimate for input signal, ***(c)*** Wavelet scale index spectrum of the Duffing oscillator: the frequency values of the weak periodic signals that are used as external forcing input in the Duffing equation correspond to near-zero wavelet scale index parameters in the graph

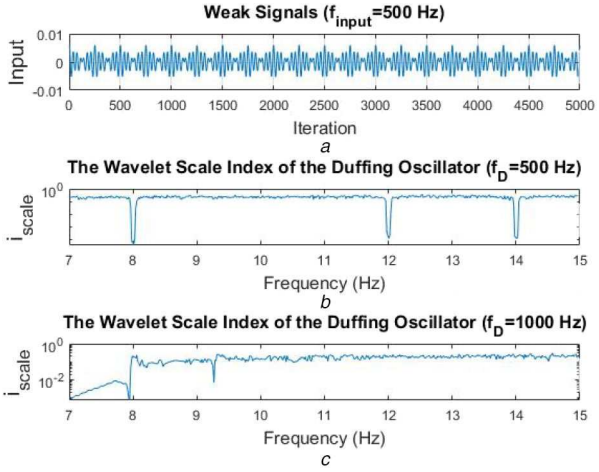

Fig. 7 *Wavelet scale index spectrum of the Duffing oscillator system with external forcing input signal*

(a) Input(τ) consists of the weak periodic signals with the frequency values of 8, 12 and 14 Hz. The sampling frequency of the input signal f_{input} is 500 Hz, ***(b)*** Sampling frequency of the oscillator was selected to be the same with the input signal, $f_{\text{D}} = f_{\text{input}}$; the weak periodic signals were detected, ***(c)*** Sampling frequency of the oscillator was selected different from the input signal, $f_{\text{D}} \neq f_{\text{input}}$; the weak periodic signal detection was not successful

The EEG signals in Figs. 8*a* and 9*a* were recorded form the scalp of two patients with the sampling rate (f_{EEG}) of 250 Hz [23].

For the application to the empirical data, the Duffing (1) can be expressed as

$$\frac{\mathrm{d}^2x}{\mathrm{d}t^2} + 0.5\frac{\mathrm{d}x}{\mathrm{d}t} - x + x^3 = \gamma\cos(\omega_0\tau) + \text{input}[\tau]_{\text{EEG}} \qquad (14)$$

Where the sampling frequency of the Duffing oscillator was selected as $f_{\text{D}} = 100/h = 100/0.1 = 1000$ Hz. According to $f_{\text{D}} = f_{\text{input}}$, the sampling frequency of the input signal was set to $f_{\text{input}} = 4f_{\text{EEG}} = 4 \times 250 = 1000$ Hz. Next, the frequency values of the weak periodic signals, detected in the EEG signals were divided by 4, $f_{\text{input}}/f_{\text{EEG}}$.

The epileptic and non-epileptic EEG time series were scaled to fit the reference signal in (14), $\text{input}_{\text{EEG}} = 10^n(\text{EEG Signals})$. For this, the rms values of the EEG signals were calculated as $(\text{epileptic EEG})_{\text{rms}} = 2320\,\mu\text{V}$ and $(\text{nonepileptic EEG})_{\text{rms}} = 218\,\mu\text{V}$. According to the inequality (13), the time series were multiplied by gain coefficients of 10^{-5} and 10^{-4}, respectively, as shown in Figs. 8*b* and 9*b*. The amplitude of the reference signal in (14) was set to $\gamma = 0.8254$, ($\gamma_{\text{c}} = 0.8255$).

The angular frequency scanning was carried out by the time step of 0.001 in the interval of $1 \leq \omega_0 \leq 1.319$. The expression of the frequency of the Duffing oscillator in terms of the angular frequency is $f = 100\omega_0/2\pi$. Thus, the selected angular frequency interval corresponds to the frequency values between 15.92 and 21.0 Hz. The wavelet scale index values of the Duffing oscillator in (14) were computed for this frequency range. Here, the Haar wavelet function with the scales between $s_0 = 1$ and $s_1 = 512$ was used. Figs. 8*d* and 9*d* show the wavelet scale index–frequency graphs of the Duffing oscillator using (14). In these graphs, the wavelet scale index parameters with near-zero values indicate the frequency values of the weak periodic signals [2, 3, 15, 23, 33]. The weak periodic signal search was carried out for $f_{\text{D}} = f_{\text{input}} = 1000$ Hz. For the EEG signals recorded with the sampling frequency of $f_{\text{EEG}} = 250$ Hz, the frequency values of the weak periodic signals were divided by 4; Fig. 8*d* shows the frequency values of the weak periodic signals in the epileptic EEG signals which are $16.84/4 = 4.21$ and $17.53/4 = 4.38$ Hz. Fig. 9*d* shows the frequency values of the weak periodic signals in the non-epileptic EEG signals which are $16.38/4 = 4.1$, $17.62/4 = 4.4$ and $19.44/4 = 4.86$ Hz. The method was also compared with the power spectral density estimate of the EEG signals as shown in Figs. 8*c* and 9*c*.

3.2.1 Measuring the amplitude of a weak periodic signal in the empirical data: Using the Duffing oscillator, the amplitude magnitude (a) of a weak periodic signal in the empirical data can be measured by changing the reference signal amplitude (γ) while the angular frequency (ω_0) is kept constant. When the total periodic amplitude in (14) is greater than or equal to the bifurcation value of the reference signal amplitude, $\gamma + a \geq \gamma_{\text{c}}$, the Duffing oscillator remains in the large-scale periodic state. Therefore, by fixing the reference angular frequency (ω_0) to a detected weak periodic signal frequency, and the reference signal amplitude (γ) is decreased to a certain value where the large-scale periodic state of the Duffing oscillator starts to deform. Thus, the amplitude value of the weak periodic signal is determined as $a = \gamma_{\text{c}} - \gamma$ [15, 23].

In Section 3.2, we selected the reference signal amplitude and the bifurcation value as $\gamma = 0.8254$ and $\gamma_{\text{c}} = 0.8255$, respectively. Also, we found the frequency of the weak periodic signal as 16.84 Hz ($\omega_0 = 1.058$) in the epileptic EEG signal for the sampling frequency of the input signal, $f_{\text{input}} = 1000$ Hz. To measure the amplitude value of the detected weak periodic signal, the reference signal amplitude value (γ) was decreased by keeping the reference angular frequency constant at $\omega_0 = 1.058$ in the Duffing (14). The large scale stable-periodic state of the Duffing oscillator deformed for the reference signal amplitude of $\gamma = 0.8243$. As a result, the amplitude value of the weak periodic signal was calculated as $a = \gamma_{\text{c}} - \gamma = 0.8255 - 0.8244 = 0.0011$. The real value of the weak periodic signal amplitude a was found by dividing with the gain coefficient, $a' = a/10^n = 0.0011/10^{-5} = 110\,\mu\text{V}$ (see Section 3.2). We followed the same procedure, to find the amplitude value of the detected weak periodic signal in the non-epileptic EEG signal as $1\,\mu\text{V}$.

4 Conclusions

Modern signal processing techniques are mainly based on the frequency-domain analysis originated from FFT. However, a simple FFT method is not capable of detecting weak periodic signals submerged in background noise, as shown in Figs. 5*b* and 6*b*. The conventional method of analysing the state space diagrams of the Duffing oscillator is effective in detecting weak periodic signals in noise with low SNR as demonstrated in Fig. 2 [7, 34–44]. However, this method is manual; it does not have a graphical representation of the frequency spectrum such as FFT.

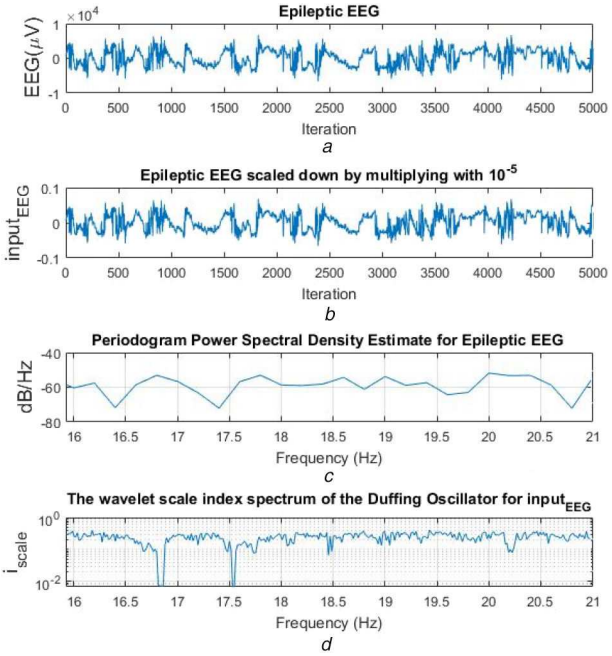

Fig. 8 *Wavelet scale index spectrum of the Duffing oscillator system with external forcing EEG signal, and periodogram power spectral density of the EEG signal*

(a) Epileptic EEG signals were recorded with the sampling rate of $f_{\text{EEG}} = 250$ Hz, ***(b)*** Epileptic EEG signals were scaled down by a gain coefficient of 10^{-5}, ***(c)*** Periodogram power spectral density estimate for the epileptic EEG signals, ***(d)*** Wavelet scale index spectrum of the Duffing oscillator: The weak periodic signals were detected within the epileptic EEG signals that were used as external forcing input in the Duffing oscillator, $f_{\text{D}} = f_{\text{input}} = 4f_{\text{EEG}} = 1000$ Hz. For $f_{\text{EEG}} = 250$ Hz, the frequency values of the weak periodic signals were found as $16.84/4 = 4.21$ and $17.53/4 = 4.38$ Hz

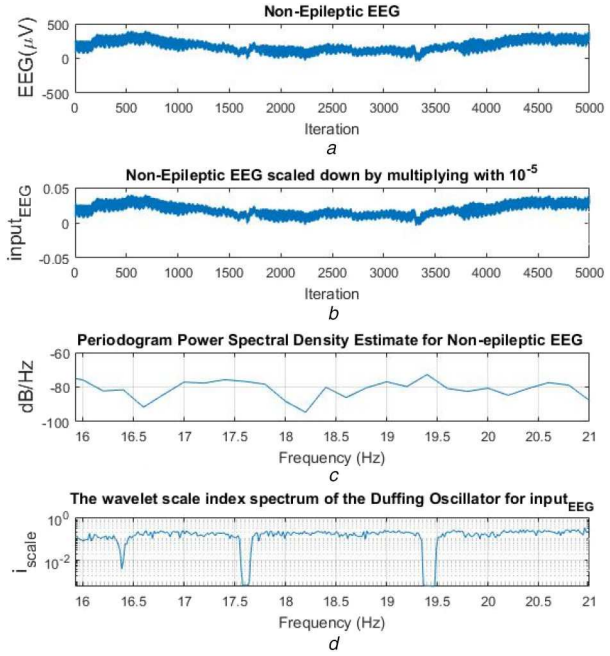

Fig. 9 *Wavelet scale index spectrum of the Duffing oscillator system with external forcing EEG signal, and periodogram power spectral density of the EEG signal*

(a) Non-epileptic EEG signals were recorded with the sampling rate of $f_{\text{EEG}} = 250$ Hz, ***(b)*** Non-epileptic EEG signals were scaled down by a gain coefficient of 10^{-4}, ***(c)*** Periodogram power spectral density estimate for the non-epileptic EEG signal, ***(d)*** Wavelet scale index spectrum of the Duffing oscillator: the weak periodic signals were detected within the non-epileptic EEG signals that were used as external forcing input in the Duffing oscillator, $f_{\text{D}} = f_{\text{input}} = 4f_{\text{EEG}} = 1000$ Hz. For $f_{\text{EEG}} = 250$ Hz, the frequency values of the weak periodic signals were found as $16.38/4 = 4.1$, $17.62/4 = 4.4$ and $19.44/4 = 4.86$ Hz

In this work, we presented a method based on the wavelet scale index analysis of the Duffing oscillator. We used the wavelet scale index parameters to numerically distinguish between the chaotic and periodic states of the Duffing oscillator. We preferred the wavelet scale index as a quantitative index in the classification of signals. As shown in Fig. 3, the wavelet scale index proves to be more sensitive than the maximum Lyapunov exponent in detecting the transition of the Duffing oscillator from the critical chaotic state to the periodic state. The wavelet scale index parameters of the Duffing oscillator converge to zero in the large-scale periodic state of the system and have values between zero and one when the system is in chaos. This feature allows us to plot the wavelet scale index–frequency graph to display the weak periodic signal search results, similar to the power spectral density graph. Thus, weak periodic signals are searched automatically by the proposed method without the need to manually analyse the state space diagrams of the Duffing oscillator.

This new approach for the weak periodic signal detection, based on the wavelet scale index spectrum of the Duffing oscillator, was performed successfully as shown in Figs. 4*c*, 5*c* and 6*c*. The simulation results showed that initially unknown frequencies of the weak periodic signals correlate with near-zero wavelet scale index parameters in the spectrum.

The application of this method in the empirical data was explained in Section 3.2. Weak periodic signals were also detected within the empirical data that were used as external forcing input in the critical chaotic state of the Duffing oscillator. First, the amplitude scale of the empirical data was fitted to the reference signal of the Duffing oscillator with a suitable gain coefficient. Then, the sampling frequency of the Duffing oscillator, f_{D} was set equal to the sampling frequency of the empirical data, f_{input}. For this, the time step size of the Duffing oscillator was determined as $h = 100/f_{\text{input}}$. Finally, the wavelet scale index spectrum of the Duffing oscillator was plotted for the frequency scanning. Near-zero wavelet scale index parameters in the spectrum correspond to the frequency values of the weak periodic signals in the empirical data, as shown in Figs. 8 and 9.

The method was performed using the two EEG signals as the external forcing input in the Duffing equation to demonstrate the feasibility in the empirical data. Here, the presence of the weak periodic signals within the EEG signals may potentially reveal more information about the dynamic structure of the brain.

This method can be used in studying the weak signals in time series of the measurable processes of dynamical systems in diverse fields [45–50]. Consequently, we understand that this method is more efficient in weak periodic signal detection compared to the conventional method that relies on state-space analysis of the Duffing oscillator.

5 References

[1] Yu, Y., Liu, F., Wang, W.: 'Frequency sensitivity in Hodgkin–Huxley systems', *Biol. Cybern.*, 2001, **84**, (3), pp. 227–235

[2] Jung, S.N., Longtin, A., Maler, L.: 'Weak signal amplification and detection by higher-order sensory neurons', *J. Neurophysiol.*, 2016, **115**, (4), pp. 2158–2175

[3] Fan, H., Wang, Y., Wang, H., *et al.*: 'Autapses promote synchronization in neuronal networks', *Sci. Rep.*, 2018, **8**, p. 580

[4] Yue, L., Bao-Jun, Y., Xue-Ping, Z., *et al.*: 'Algorithm of chaotic vibrator to detect weak events in seismic prospecting records', *Chin. J. Geophys.*, 2005, **48**, (6), pp. 1428–1433

[5] Li, Y., Yang, B.J., Badal, J., *et al.*: 'Chaotic system detection of weak seismic signals', *Geophys. J. Int.*, 2009, **178**, (3), pp. 1493–1522

[6] Sun, M., Li, Z., Li, Z., *et al.*: 'A noise attenuation method for weak seismic signals based on compressed sensing and CEEMD', *IEEE Access*, 2020, **8**, pp. 71951–71964

[7] Li, G., Tan, N., Li, X.: 'Weak signal detection method based on the coupled Lorenz system and its application in rolling bearing fault diagnosis', *Appl. Sci.*, 2020, **10**, p. 4086

[8] Wang, Q.B., Yang, Y., Zhang, X.: 'Detection of weak signal based on parameter identification of delay differential system with noise disturbance', *Math. Probl. Eng.*, 2020, Article ID 2047952, p. 9, https://doi.org/10.1155/2020/2047952

[9] Luo, J., Xu, X., Ding, Y., *et al.*: 'Application of a memristor-based oscillator to weak signal detection', *Eur. Phys. J. Plus*, 2018, **133**, p. 239

[10] Kumar, S., Jha, R.K.: 'Weak signal detection using stochastic resonance with approximated fractional integrator', *Circuits Syst. Signal Process.*, 2019, **38**, pp. 1157–1178

[11] Wang, G., Chen, D., Lin, J., *et al.*: 'The application of chaotic oscillators to weak signal detection', *IEEE Trans. Ind. Electron.*, 1999, **46**, pp. 440–444

[12] Wang, G.Y., He, S.L.: 'A quantitative study on detection and estimation of weak signals by using chaotic duffing oscillators', *IEEE Trans. Circuits-I*, 2003, pp. 945–953

[13] Zeng, L., Zhang, L.: 'State identification of duffing oscillator based on extreme learning machine', *IEEE Signal Process. Lett.*, 2018, **25**, (1), pp. 25–29

[14] Luo, W.M., Zhang, Y.R.: 'Non-periodic pulse signal detection based on variable scale coupled Duffing oscillators', *Electron. Lett.*, 2018, **54**, (5), pp. 280–281

[15] Akilli, M.: 'Detecting weak periodic signals in EEG time series', *Chin. J. Phys.*, 2016, **54**, pp. 77–85

[16] Han, X., Bi, Q.: 'Bursting oscillations in Duffing's equation with slowly changing external forcing', *Commun. Nonlinear Sci. Numer. Simul.*, 2011, **16**, pp. 4146–4152

[17] Han, X., Yub, Y., Zhangc, C., *et al.*: 'Turnover of hysteresis determines novel bursting in Duffing system with multiple-frequency external forcings', *Int. J. Non-Linear Mech.*, 2017, **89**, pp. 69–74

[18] Han, X., Zhang, Y., Bi, Q., *et al.*: 'Two novel bursting patterns in the Duffing system with multiple- frequency slow parametric excitations', *Chaos*, 2018, **28**, p. 043111

[19] Niu, J., Liu, R., Shen, Y., *et al.*: 'Chaos detection of Duffing system with fractional-order derivative by Melnikov method', *Chaos*, 2019, **29**, p. 123106

[20] Wang, K., Yan, X., Yang, Q., *et al.*: 'Weak signal detection based on strongly coupled Duffing-Van der Pol oscillator and long short-term memory', *J. Phys. Soc. Jpn.*, 2020, **89**, p. 014003

[21] Benitez, R., Bolos, V.J., Ramirez, M.E.: 'A wavelet based tool for studying non-periodicity', *Comput. Math. Appl.*, 2010, **60**, pp. 634–641

[22] Bolós, V.J., Benitez, R., Ferrerc, R., *et al.*: 'The windowed scalogram difference: a novel wavelet tool for comparing time series', *Appl. Math. Comput.*, 2017, **312**, pp. 49–65

[23] Akilli, M., Yilmaz, N.: 'Study of weak periodic signals in the EEG signals and their relationship with postsynaptic potentials', *IEEE Trans. Neural Syst. Rehabil. Eng.*, 2018, **26**, (10), pp. 1918–1925

[24] Akilli, M., Yilmaz, N., Akdeniz, K.G.: 'Study of the q-Gaussian distribution with the scale Index and calculating entropy by normalized inner scalogram', *Phys. Lett. A*, 2019, **383**, (11), pp. 1099–1104

[25] Yilmaz, N., Canbaz, B., Akilli, M., *et al.*: 'Study of the stability of the fermionic instanton solutions by the scale index method', *Phys. Lett. A*, 2018, **382**, (32), pp. 2118–2121

[26] Yilmaz, N., Akilli, M., Özbek, M., *et al.*: 'Application of the nonlinear methods in pneumocardiogram signals', *J. Biol. Phys.*, 2020, **46**, pp. 209–222

[27] Kovacic, I., Brennan, M.J.: '*The duf_ng equation: nonlinear oscillators and their behaviour*' (Wiley, Chichester, UK, 2011)

[28] Peng, H.-H., Xu, X., Yang, B.-C., *et al.*: 'Implication of two-coupled differential Van der Pol duffing oscillator in weak signal detection', *J. Phys. Soc. Jpn.*, 2016, **85**, (4), p. 8

[29] Griffiths, D.F., Higham, D.J.: '*Numerical methods for ordinary differential equations*' (Springer-Verlag, London, 2010)

[30] Mallat, S.: '*A wavelet tour of signal processing*' (Academic Press, London, 1999)

[31] Balcerzak, M., Pikunov, D., Dabrowski, A.: 'The fastest, simplified method of Lyapunov exponents spectrum estimation for continuous-time dynamical systems', *Nonlinear Dyn.*, 2018, **94**, pp. 3053–3065

[32] Zeni, A.R., Gallas, J.A.C.: 'Lyapunov exponents for a Duffing oscillator', *Physica D*, 1995, **89**, pp. 71–82

[33] Liu, F., Wang, J.F., Wang, W.: 'Frequency sensitivity in weak signal detection', *Phys. Rev. E*, 1999, **59**, p. 3453

[34] Wanga, G., Zhenga, W., He, S.: 'Estimation of amplitude and phase of a weak signal by using the property of sensitive dependence on initial conditions of a nonlinear oscillator', *Signal Process.*, 2002, **82**, (1), pp. 103–115

[35] Duan, F., Chapeau-Blondeau, F., Abbott, D.: 'Noise-enhanced SNR gain in parallel array of bistable oscillators', *Electron. Lett.*, 2006, **42**, (17), pp. 1008–1009

[36] Duan, F., Chapeau-Blondeau, F., Abbott, D.: 'Non-Gaussian noise benefits for coherent detection of narrowband weak signal', *Phys. Lett. A*, 2014, **378**, (26–27), pp. 1820–1824

[37] Zhang, X., Yan, J., Duan, F.: 'Comparison of bistable systems and matched filters in non Gaussian noise', *Fluctuation Noise Lett.*, 2016, **15**, (1), p. 1650003

[38] Lai, Z.-H., Leng, Y.-G.: 'Generalized parameter-adjusted stochastic resonance of Duffing oscillator and its application to weak-signal detection', *Sensors*, 2015, **15**, (9), pp. 21327–21349

[39] Duan, F.B., Chapeau-Blondeau, F., Abbott, D.: 'Weak signal detection: condition for noise induced enhancement', *Digit. Signal Process.*, 2013, **23**, pp. 1585–1591

[40] Alfonsi, L., Gammaitoni, L., Santucci, S., *et al.*: 'Intrawell stochastic resonance versus interwell stochastic resonance in underdamped bistable systems', *Phys. Rev. E*, 2000, **62**, pp. 299–302

[41] Wang, Y., Xu, G., Zhang, S., *et al.*: 'EEG signal co-channel interference suppression based on image dimensionality reduction and permutation entropy', *Signal Process.*, 2017, **134**, pp. 113–122

[42] Wang, G., Zhu, J., Xu, Z.: 'Asymptotically optimal one-bit quantizer design for weak-signal detection in generalized Gaussian noise and lossy binary communication channel', *Signal Process.*, 2019, **154**, pp. 207–216

[43] Zhu, Q., Lin, F., Li, H., *et al.*: 'Human-autonomous devices for weak signal detection method based on multimedia chaos theory', *J Ambient Intell. Human Comput.*, 2020, https://doi.org/10.1007/s12652-020-02270-x

[44] Zhang, L., Ji, Y., Luo, M.: 'Parameter estimation of weak signal based on the steady attractor of duffing oscillator', *Chin. J. Electron.*, 2019, **28**, (4), pp. 781–788

[45] Yu, M., Zhang, G., Li, Q., *et al.*: 'PGMM—pre-trained Gaussian mixture model based convolution neural network for electroencephalography imagery analysis', *IEEE Access*, 2020, **8**, pp. 157418–157426

[46] Vink, J.J.T., Klooster, D.C.W., Ozdemir, R.A., *et al.*: 'EEG functional connectivity is a weak predictor of causal brain interactions', *Brain Topogr.*, 2020, **33**, pp. 221–223

[47] Zheng, X., Chen, W., You, Y., *et al.*: 'Ensemble deep learning for automated visual classification using EEG signals', *Pattern Recognit.*, 2020, **102**, p. 107147

[48] Dohnal, G.: 'Weak signal detection in SPC', *Appl. Stoch. Models. Bus. Ind.*, 2020, **36**, (2), pp. 225–236

[49] Masoliver, M., Masoller, C.: 'Neuronal coupling benefits the encoding of weak periodic signals in symbolic spike patterns', *Commun. Nonlinear Sci. Numer. Simulat.*, 2020, **82**, p. 105023

[50] Kalra, M., Kumar, S., Das, B.: 'Moving ground target detection with seismic signal using smooth Pseudo wigner–ville distribution', *IEEE Trans. Instrum. Meas.*, 2020, **69**, (6), pp. 3896–3906